INTERNATIONAL JOURNAL OF MARITIME TECHNOLOGY
IJMT Vol.13/ Winter 2020 (51-59)
Available online at: www. ijmt.ir

Hydroelastic Analysis of Composite Marine Propeller Basis Fluid-Structure Interaction (FSI)

Amir Arsalan Shayanpoor[1], Ahmad Hajivand [2*], Masih Moore[3]

[1] *BSc, Khorramshahr University of Marine Science and Technology; arsalan.shayanpoor@gmail.com*
[2*] *Faculty of Marine Engineering Department, Khorramshahr University of Marine Science and Technology; hajivand@kmsu.ac.ir*
[3] *Faculty of Marine Engineering Department, Khorramshahr University of Marine Science and Technology; m.moore@kmsu.ac.ir*

ARTICLE INFO

Article History:
Received: 22 Dec. 2019
Accepted: 01 Aug. 2020

Keywords:
Hydroelastic
Composite propeller
Hydrodynamic performance
FSI

ABSTRACT

In recent decades, there has been a growing demand for composite materials with high strength to weight ratio and high stiffness to weight ratio for use in the marine industry to improve the hydrodynamic and structural performance of vessels and propulsion systems. Apart from the advantages of composite propellers over their metal counterparts, deformations of these propellers under loading can alter their hydrodynamic effects. This paper was a hydroelastic analysis of a composite marine propeller made of carbon fiber laminate. This analysis was performed by the use of CFD-FEM based on the two-way fluid-structure interaction (FSI) coupling on the 3D geometry of the KP458 propeller. The CFD results are compared with the experimental data reported by Hyundai Maritime Research Institute (HMRI), for advance ratios of 0.1-0.5, which shows a perfect agreement among them. An increase in the efficiency of the flexible propeller is observed in different advance ratios due to an increase in thrust (1-4%) and a decrease in torque (1-6%).

1. Introduction

Composite marine propellers have various advantages over conventional alloy propellers, Such as higher strength to weight ratio and toughness, lower lifetime maintenance cost, immunity to corrosion and cavitation damage, better acoustic damping, lower noise and vibration, no magnetic signature, superior fatigue performance and shape adaptability [1-3]. Thanks to these hydrodynamic, structural, and environmental benefits, composite materials have extensive use in the marine industry. It is possible to fabricate propeller blades from a composite of resin and fibers to reduce the cavitation effect (up to 70%) [4]. In addition to reducing cavitation damage, composite materials can also improve corrosion resistance, fatigue and damping performance [5]. Also, composite propellers are typically 1.5 times lighter than nickel-aluminum-bronze (NAB) propellers, a difference that can reduce ship noise by 10-90%, decrease fuel consumption during operation, and increase open water efficiency by 3-8%. Therefore, composite materials generally outperform propellers made of materials such as NAB and manganese-nickel-aluminum-bronze (MAB) [6]. However, due to the anisotropic behavior of the composite materials, the created hydroelastic effects can affect the hydrodynamic performance of the propeller.

Over the years, many researchers have studied the use of composite materials in the marine propellers and different numerical methods such as lifting surface method (LSM), finite element method (FEM), computational fluid dynamics (CFD), vortex-lattice method (VLM) and boundary element method (BEM) have been developed and used to predict propeller performance. Rao et al. [7] used the finite element method to analyze the stress in a marine composite propeller to reduce stresses in stiffer composite propellers. In a study by Lin [8], the strength of composite propeller blades was examined using LSM-FEM with shell elements. This study also examined the strength of the blades with balanced and unbalanced ply- stacking. Ultimately, this study concluded that the propeller blade with […/-45º/90º/0º] ply-stacking does not exhibit sufficient strength, but those with […/θ_2 /90º/0º] and […/-15º/15º/90º/0º] lamination provide a desirable strength. Pavan Kishore et al. [9] conducted a structural analysis on a composite propeller to be used as a replacement for an aluminum propeller. Their results showed that optimizing the stacking of the composite propeller can result in higher stiffness. Ghassemi et al. [10] carried out a

hydrostructural analysis on a composite propeller under hydrodynamic pressure. A BEM-FEM method was used to evaluate the hydrodynamic performance of a B-Series propeller, and then the governing equations were solved based on RANS equations. Paik et al. [11] conducted a numerically and experimentally study of different composite propellers. Lee et al. [12] developed a BEM-FEM hydroelastic method to predict performance of a flexible composite marine propeller. Hong et al. [13] developed a pre-twist strategy based on a coupled FEM/CFD process, using the general-purpose software ANSYS/CFX, to improve hydrodynamic performance.

Han et al. [14] applied an experimentally validated CFD-FEM FSI technique to study the advantages of composite marine propellers using Star-CCM+ and Abaqus Co-simulation. Das and Kapuria [15] considered the utilization of bend–twist coupling of a composite marine propeller for improved hydrodynamic properties. Hong et al. [16] applied a 3-D FEM/CFD coupling algorithm to examine the hydrodynamic, structural deformation, and cavitation performance of the 438x series of composite propeller. Kumar et al. [17] design and evaluated a composite marine propeller for a pod propulsor.

Zhang et al. [18] applied the commercial software ANSYS Workbench to study a large screw seven-bladed composite propeller's hydrodynamic and structural performance. Their results showed that the effects of FSI in the analysis of flexible composite propellers should be considered.

Vijayanandh et al. [19] predicted the fatigue life of two naval propeller using numerical simulation with one way coupled environments. Also, they applied the coupled FSI analyses for various existing materials such as Aluminum alloy, Stainless Steel.

Summarizing the researches show that due to the lower strength of the impeller than the metal, these impellers will undergo significant deformation due to the hydrodynamic pressure of the water and, at the same time, the deformed impeller will affect the fluid movement and distribution of hydrodynamic loads.

This issue highlights:

Based on the mentioned outstanding studies, the importance of hydroelastic analyses that estimate deformed propellers' efficiency has been highlighted. Accordingly, this paper will further examine the hydroelastic performance of a composite propeller. For this purpose, the advanced fluid flow and structural 3D solvers have been used. Besides, FSI analysis has been performed by the co-simulation technique that allows fluid and structure solvers to exchange data more than once per time-step. To validate the developed numerical model, the benchmark four-bladed FPP propeller KP458 has been used. This propeller model with small skew, was designed in 1959 and was tested by INSEAN (Instituto Nazionale di Studi ed Esperienze di Architettura Navale) in non-cavitating conditions.

In addition, a comparison was made between the two common methods for treating the propeller motion: sliding mesh and MRF. Also, two types of volume mesh were compared: polyhedral and hexahedral (trimmer). An implicit coupling scheme has been used to perform the FSI coupling iteration process. A diagram of the method used for analysis is illustrated in Fig. 1.

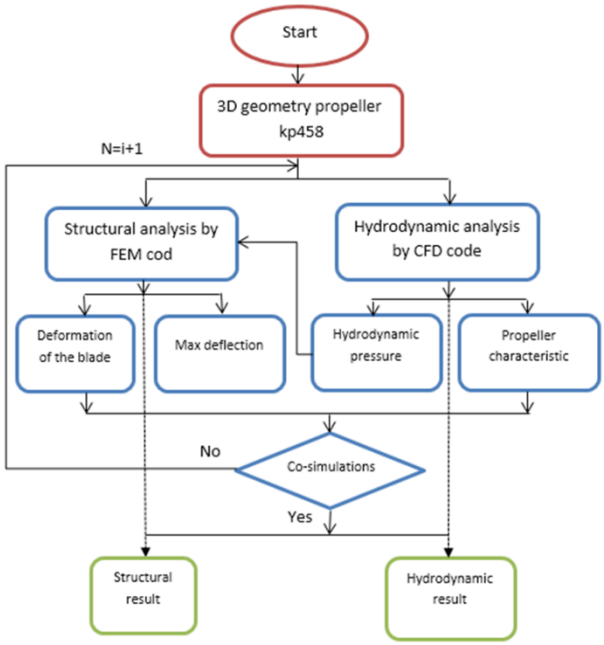

Figure. 1: Schematic diagram of the FSI coupling iteration process;

2. Numerical model

To accomplish hydroelastic study for the performance evaluation of a composite propeller a numerical model is created based on the CFD/FEM process. The two-way fluid-structure coupling calculation of flexible propeller is performed in the software STAR-CCM+ and structural computation module in Abaqus. The FSI calculation model is constituted of the flexible propeller model and the external flow field model. The two-way FSI technique is used to realize the transfer of fluid pressure and structural deformation data in the coupling process.

2.1. Propeller model description

The open water test simulation is performed for the propeller KP458 model, as shown in Fig 2, which is designed by the MOERI for the KVLCC2 model tanker. The design parameters and details of the propeller model are also given in Table 1 and Table 2, respectively.

Table 1. design parameters of the propeller KP458 model;

Type	FP
Scale	110
No. of blades	4
D (m)	0.0896
P/D (0.7R)	0.721
Ae/A0	0.431
Rotation	Right hand
Hub ratio	0.155

Table 2. Propeller geometry properties;

r/R	P/D	X_m/D	Skew(deg)	C/D	f_0/C	t_0/D
0.16	0.5765	0	-2.53	0.1515	0.0313	0.0468
0.25	0.613	0	-4	0.1772	0.0349	0.0422
0.3	0.631	0	-4.4	0.1892	0.0356	0.0385
0.4	0.663	0	-4.4	0.2093	0.0338	0.032
0.5	0.6915	0	-3.15	0.2247	0.0293	0.026
0.6	0.712	0	-0.82	0.2335	0.025	0.0206
0.7	0.7212	0	2.49	0.2338	0.0219	0.0156
0.8	0.716	0	6.35	0.2192	0.0198	0.0111
0.9	0.6927	0	10.76	0.1808	0.0161	0.007
0.95	0.6748	0	13.15	0.1422	0.0128	0.0047
1	0.651	0	16.75	0	0	0.0032

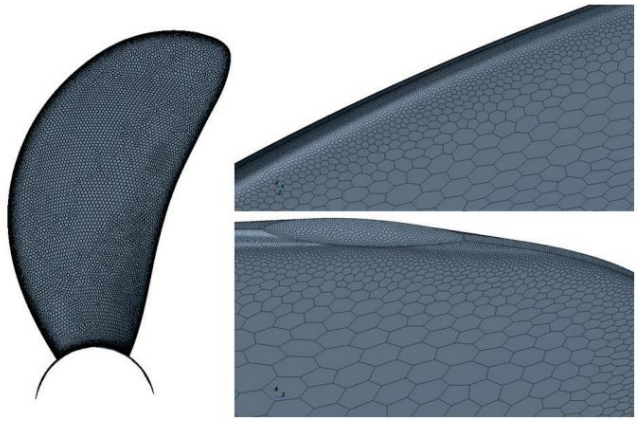

Figure. 2 KP458 model geometry;

2.2. Fluid analysis method

The equations best suited for describing an unsteady viscous turbulent incompressible flow around a ship are continuity and Navier-Stokes (NS) according to Eq. (1).

$$\frac{\partial U_i}{\partial X_i} = 0$$
$$\rho \frac{\partial U_i}{\partial t} + \rho U_l \frac{\partial U_i}{\partial X_l} = -\frac{\partial P}{\partial X_i} + \frac{\partial}{\partial X_l}\left(\mu \frac{\partial U_i}{\partial X_l} - \overline{\rho U_\iota U_l}\right) \quad (1)$$

Where $U_i = (U, V, W)$ is the vector of velocity in the direction X_i(x, y, z), ρ is density, P is pressure, μ is the dynamic viscosity of the fluid, and $\overline{\rho U_\iota U_l}$ is Reynolds stress. The SST $k-\omega$ turbulence model was used to model the formed eddies near the propeller while rotating. This two-equation turbulence model switches adaptively between $k-\omega$ model inside the boundary layer and the $k-\varepsilon$ model in the free stream. It also provides a good compromise between precision, computational effort, and robustness.

In the open water experiment, the water flow is uniform and symmetrical. Therefore, numerical solution is carried out using the moving reference frame (MRF) technique with alternating boundary conditions, under the real operating conditions that inflow is non-uniform and propeller is placed at the stern of the ship.

2.3. Solid analysis method

The equation of motion is expressed relative to a propeller blade fixed coordinate to consider the structural deformation

$$M_s\ddot{d} + C_s\dot{d} + K_s d = F_{ST}$$
$$F_{ST} = F_{hp} + F_{cori} + F_{cent} + F_{fs} = F_s + F_{fs} \quad (2)$$

Where M_s is the mass coefficient, C_s is the damping coefficient, and K_s is the stiffness coefficient, which depend on the mass, damping, and stiffness of the composite propeller. The parameters d, $\dot{d}$, and $\ddot{d}$ denote the displacement, velocity, and acceleration of the structure, respectively, and F_{ST} is the resultant of all forces applied to the propeller, including the hydrodynamic pressure F_{hp}, the Coriolis force, F_{cori}, the centrifugal force F_{cent}, and the structure-fluid interaction force F_{fs}.

The structural qualities of composite materials depend on the type and stacking sequence of ply lamination. However, it is difficult to design a propeller by direct analysis because this approach would require long and sophisticated computations resulting from the use of detailed meshes and 3D geometric models. In this research, the continuum shell element (S8R) element of Abaqus software was used to reduce the meshing computations. This element is a good choice for the analysis of composite laminates in the direction of their thickness. For example, knowing the thickness of the element and the thickness of the composite plies, the entire composite laminate can be modeled with one element. This modeling approach can be widely applied to all elements of the propeller.

The validity of this modeling approach has been evaluated by Lee et al. [5] by compared the results obtained for a composite cantilever beam modeled with this approach, and the same beam modeled with real lay-up of composite plies meshing. The results showed that this simple model is useful for hydroelastic analysis of composite marine propellers because the deformation difference is insignificant and is within the error range of the FSI analysis.

2.4. Fluid structure interaction method

In FSI simulation, to solve the flow equation, we need to have surface deformations of the structure, and for structural analysis, we need to have the shear stress at the fluid-structure interface. For displacement, the conditions are as follows:

$$d_s = d_f$$
$$Tr_s = Tr_f$$
$$Tr_f = p_f n_f - \sigma_f n_f$$
$$Tr_s = \sigma_s n_s \quad (3)$$

Where d is the displacement of the structure interface, T_r is the tensile force vector, P is the fluid pressure, n is the normal vector, and σ is the stress vector.
Fluid structure interaction analysis for composite propeller is performed by the co-simulation technique and an implicit coupling scheme that allows fluid and structure solvers exchange data more than once per time-step.

3. Application of the simple ply stack FE model

To assess the reliability of CFD-FEM analysis, the test results obtained for a flexible vertical plate elastic flap that is pinned at the base [21] under a uniform flow with Re =1600 were compared with the results of the numerical solution obtained from STAR-CCM and Abaqus using the SST k-ω turbulence model [22]. The discretized computational domain in shown in Fig. 3 results of this comparison are presented in Fig. 4 and Table 3. Here, C_D is the drag coefficient of the deformed plate and D_x and D_z are plate displacements along the x-axis and z-axis [21]. As can be seen, the results of FSI are very close to the experimental fluid dynamic (EFD) data.

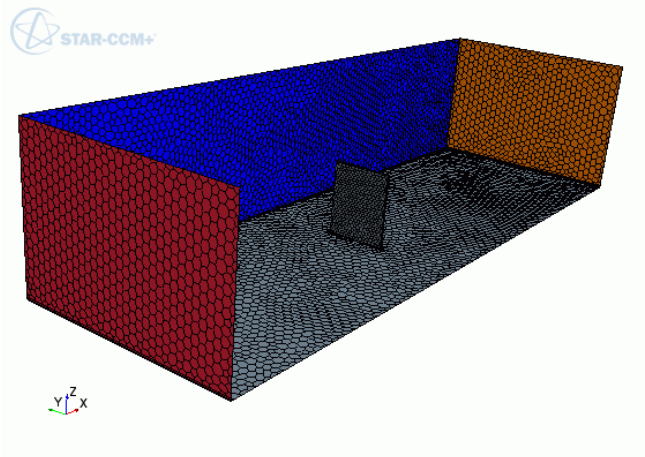

Figure. 3. Computational domain discretization by polyhedral mesh;

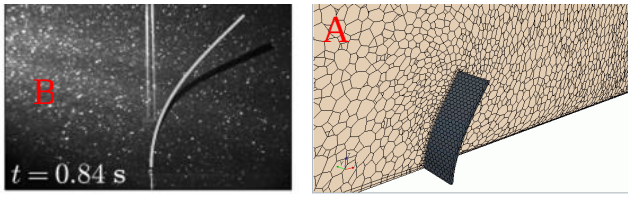

Figure. 4. bending of flexible plate in cross flow. FSI (A), EFD data (B);

Table 3. Comparison between the result and the EFD data;

	Experimental [21]	Numerical	Error %
C_D	1.15	1.11	3.47
D_x	2.14	2.19	-2.33
D_z	0.56	0.59	-5.35

In Fig. 5 the displacement plot of the inner and outer part of the top of the plate is shown vs. simulation time.

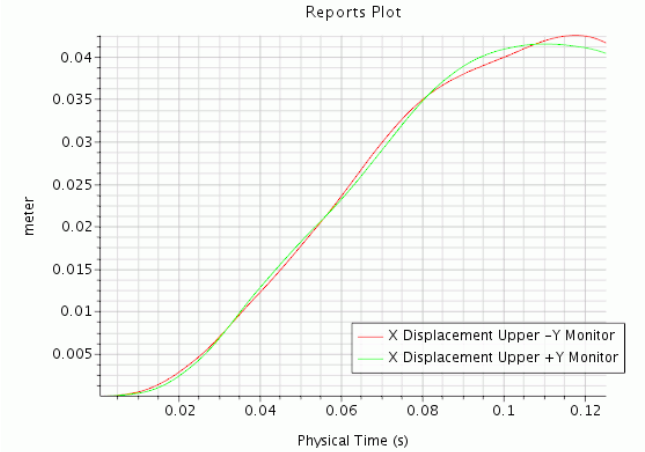

Fig. 5 The displacement plot of the inner and outer part of the top of the plate;

Therefore, the results of the hydroelastic analysis of the vertical plate can be attributed to a composite propeller that acts as a cantilever, except that the propeller has additional rotational speed. This indicates that the results of the hydroelastic analysis of composite propeller are reliable.

4. Numerical setup

Generally, there have developed various methodologies for treating the propeller motion. Out of this, the MRF and sliding strategies are the most typically utilized.
The MRF is a simple, robust, and efficient steady-state CFD modeling method to simulate a marine propeller. In this method, the governing equations solved using a rotating framework and additional terms considered in the momentum equation. But the sliding mesh is a full transient method that involves mesh motion and simulates the actual propeller rotation.
Using the MRF technique instead of sliding mesh reduces the computational effort and can provide more robust results. To compare the accuracy and the

computational time of these two methods, the open water test was simulated at different advance speeds.
Fig 6. shows hexahedral and polyhedral grid distribution around the KP458 propeller model for sliding and MRF methods, respectively. Hexahedral and In Table 4, the thrust coefficient obtained with two hard and easy methods is presented and has been compared with experimental data.

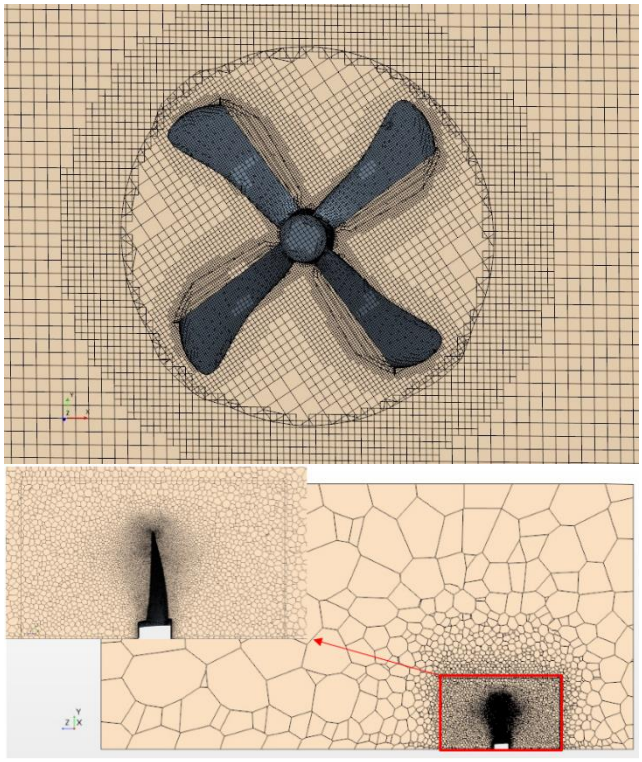

Figure. 6. Grid distribution for sliding mesh (up) and MRF method (down);

Table 4. Thrust coefficient for CFD and experimental results;

J	Sliding mesh	MRF	Experimental [23]
0.1	*0.2538*	*0.2503*	*0.2654*
0.3	*0.1852*	*0.1877*	*0.1994*
0.5	*0.1094*	*0.1077*	*0.1173*
0.6	*0.0625*	*0.0611*	*0.0756*

An examination of the results of Table 4 shows that there is not much difference between the results of the two methods. Besides, since the sliding approach is unsteady, its convergence time averages 70% more than the MRF method. For this reason, the final simulations were performed by the MRF method.
However, regarding the mesh type used, although both hexahedral and polyhedral are computationally efficient and accurate, polyhedral is much better compatible with the structural part.

5. Verification and validation

Since a numerical simulation can contain a number of errors, it is essential to evaluate the precision of the results by performing suitable verification and validation. The verification process for grid study is performed by means of three different solutions that are systematically and successively refined through constant non-integer refinement ratio r= $\sqrt{2}$ (ITTC procedures and guidelines [24]). The thrust coefficient is also subjected to verification analysis. To analyze changes in solutions, convergence ratio is defined as follows:

$$R = \frac{\varepsilon_{21}}{\varepsilon_{32}} \tag{4}$$

Where ($\varepsilon_{21} = S_2 - S_1$) is change between medium-fine solutions and ($\varepsilon_{32} = S_3 - S_2$) represents variations between coarse-medium solutions. Accordingly, the possible convergence states are:
R >1: Monotonic divergence
R < 0: Oscillatory convergence
0 < R < 1: Monotonic convergence
To evaluate grid convergence, the open water test is simulated at J=0.5 with three different meshes (g1, g2, and g3) and different grid base sizes. The solutions obtained with g1 (fine mesh), g2 (medium mesh), and g3 (sparse mesh) are also designated as S1, S2 and S3, respectively. The base size, grid numbers, and computed thrust coefficient are presented in Table 5. Moreover, convergence ratio values for different parameters are illustrated in the same Table. As well, three grid meshes are compared in Fig. 7.

Table 5. Thrust coefficient for fine, medium and coarse mesh;

Grid base size(m)	Number of grid points	Thrust coefficient
0.007	*1,111,194*	*0.1075*
0.010	*581,684*	*0.1078*
0.014	*303,036*	*0.1085*

The obtained R values represent the monotonic convergence of all parameters. In such conditions, generalized RE can also be used to estimate the order of uncertainty along with error of the results. The order of accuracy and GCI are defined as follows:

$$P = \frac{\ln\left(\frac{\varepsilon_{32}}{\varepsilon_{21}}\right)}{\ln(r)} \tag{5}$$

$$GCI = F_S \frac{|\varepsilon_{21}|}{r^P - 1} \tag{6}$$

Wherein, FS is a safety factor. FS is also set to 1.25 for conservative grid analysis with a minimum of three grids. As well, GCI represents how far off the calculated values are from the exact value. GCI method has been recommended by the American society of mechanical engineers (ASME) and the American institute of aeronautics and astronautics (AIAA). The theoretical value for the order of accuracy is P_{th}= 2. The

difference is due to grid orthogonally, problem nonlinearities, as well as turbulence modeling. The computed order of discretization and GCI values are presented in Table 6.

Table 6. *R*, *P* and *GCI* for different mesh;

Grid ratio	*R*	*P*	*%GCI*
1.414	*0.428*	*2.518*	*0.00028*

It is seen that the average difference between fine and medium spatial discretization is negligible. However, the fine grid is applied through the simulations to attain results with maximum accuracy.

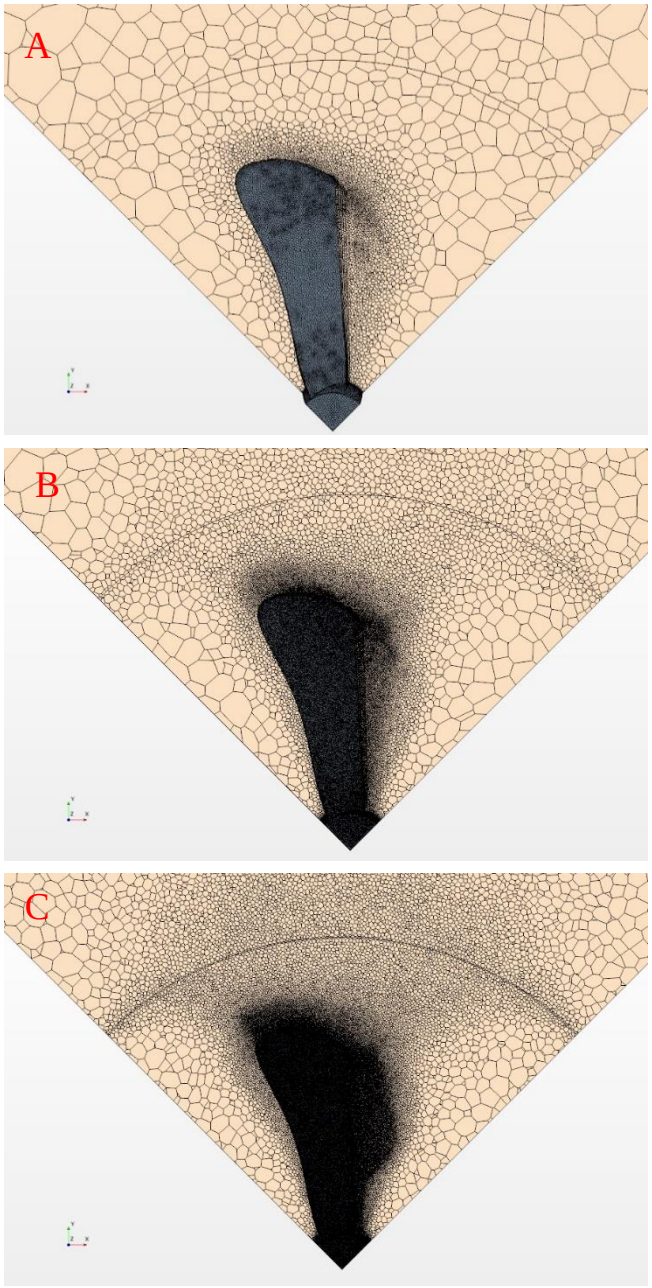

Figure. 7. Coarse mesh (A), medium mesh (B) and fine mesh (C);

6. Simulation Results

This section describes the numerical resolution settings. Between numerical algorithms, finite volume method and finite element method are straight and general techniques and have unique advantages for fluid flow and structure problems, respectively. The hydroelastic analysis was performed on the KP458 propeller model. The extents of domain boundaries for openwater simulation is cylindrical (Fig. 8), and its dimensions are set according to the ITTC recommendations [25]. To reduce computing time, only a blade passage with periodic boundary condition has been modeled.

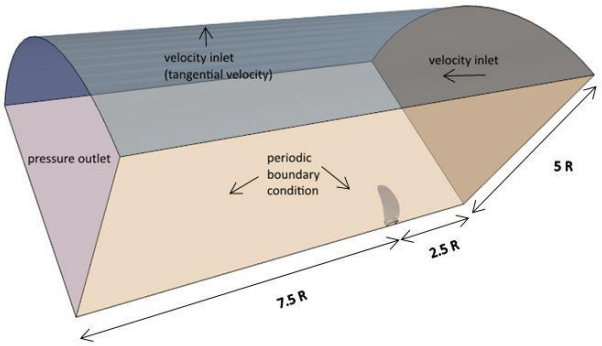

Figure. 8. Geometry of computational domain of KP458;

In Abaqus, the material considered for the composite propeller was carbon fiber with the following properties: E_1=117Gpa, E_2=7.8Gpa, υ=0.32, G_1=4.66Gpa, G_2=4.66Gpa. The reference angle (α) was 0° and the fiber orientation was [-30º/30º/0º/0º/30º/-30º] [20]. The definitions of the reference angle (α) and the fiber orientation angle relative to the reference line (θ) are provided in Fig 9.

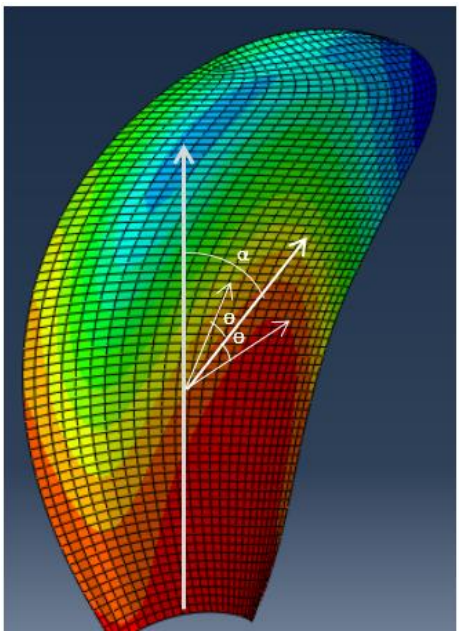

Figure. 9. Definition of the orientation angle (α) and ply angle (θ);

The modeling was performed by the use of approximately 1 million polyhedral elements for fluid analysis and 6400 S8R elements for the propeller structure. In this simulation, water density was considered to be 997.99 kg/m3 and dynamic viscosity was assumed to be 0.001409pa-s. The KP458 propeller was modeled on a scale of 1/110 (MOERI) with a diameter of 0.0896, a rotational speed of 5.244 rps, and an advance ratio of 0.1-0.6. The dimensionless number y^+ at the blade surface was 0.1-5 (Fig. 10). The time increment the structural solution was 0.1s, however, Abaqus was set to automatically improve it for better convergence. The effect of Coriolis and centrifuge forces was applied to all elements. Other solution conditions are listed in Table 6. The deformation of the propeller geometry at an advance ratio of 0.5 after 6 seconds is shown in Fig. 11.

Table 6. Co-Simulation configuration of KP458;

conditions	
Numerical	Spatial 2nd order convection Implicit dual time stepping with dt= 0.1s and 10 inner iteration K-w SST turbulence model with all y +wall treatment
Mesh	Polyhedral mesh y^+ of blade surface = 0.1 ~ 5 MRF meshing technique
FSI	STAR-CCM+ co-simulation mapping Mesh morphing method Time increment 0.1

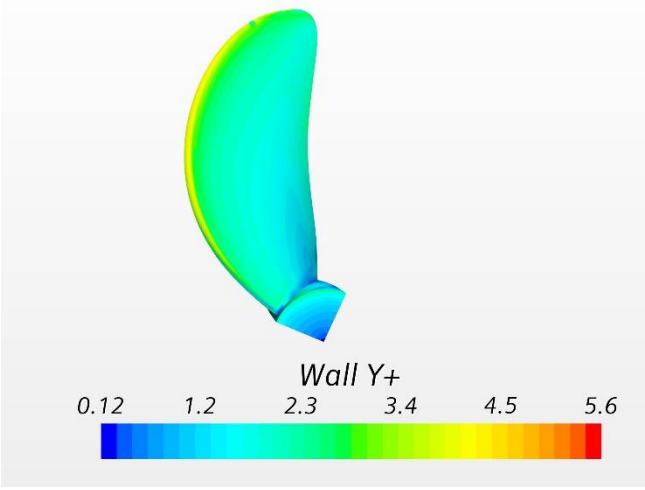

Figure. 10. Wall y^+ distribution on the propeller blade at J=0.5;

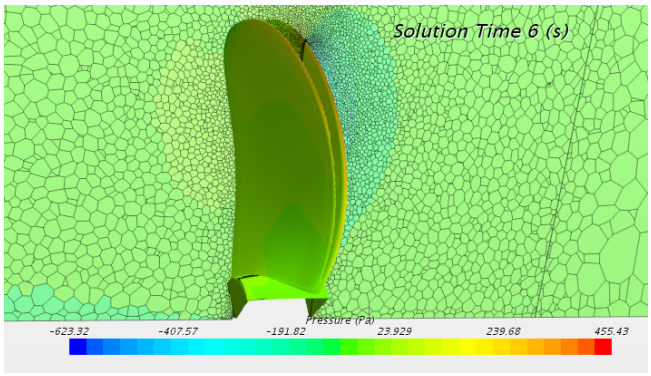

Figure. 11. Propeller shape deformation at J=0.6

It should be noted that the coefficients extracted from the simulation are based on Eq. (7) which is related to open water conditions.

$$J = V/nD$$
$$K_T = T/\rho n^2 D^4$$
$$K_Q = Q/\rho n^2 D^5$$
$$\eta_o = J.K_T/2\pi K_Q \quad (7)$$

In Fig. 12 and Table 7, CFD results of thrust coefficient, torque coefficient and open water efficiency for rigid propeller are compared with the experimental results reported by Hyundai maritime research institute (HMRI) [23]. As can be seen, the CFD results are basically consistent with the EFD results especially for advance ratios of 0.1-0.5, where errors are controlled within 2%.

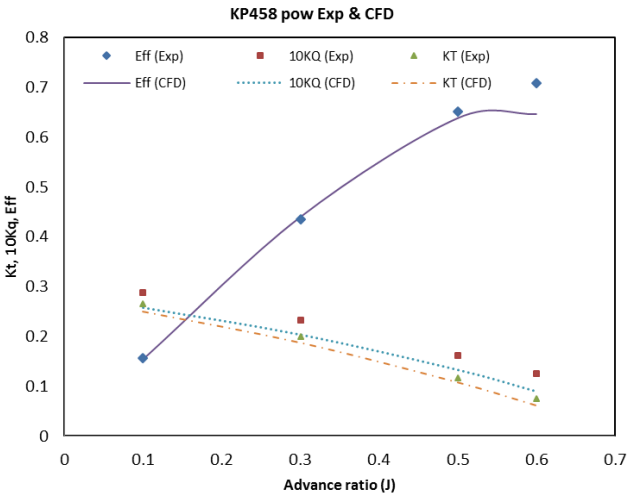

Figure. 12. Comparison of the hydrodynamic performances of KP458 POW rigid propeller (CFD) and EFD (HMRI [23]).

Table 7. Difference between experimental and CFD values of KP458 (POW) test;

J	Exp			CFD			Error of
	KT (Exp)	10KQ (Exp)	Eff (Exp)	KT (CFD)	10KQ (CFD)	Eff (CFD)	Eff %
0.1	0.2654	0.2876	0.156	0.2503	0.2575	0.1545	-0.96%
0.3	0.1994	0.2335	0.436	0.1877	0.2035	0.44	0.92%
0.5	0.1173	0.1614	0.652	0.1077	0.1333	0.6383	-2.12%
0.6	0.0756	0.1252	0.709	0.0611	0.0902	0.6465	-4.12%

Fig. 13 presents the results of CFD-FEM alongside the experimental data. The relative error variation in

different advanced ratio (J) are showed in Table 8 which, with increases J the difference between experimental and CFD-FEM values increases up to 8.88%. Fig. 11 shows an increase in the efficiency of the flexible propeller, which is due to increased thrust and reduced torque. There is about 1-4% change in thrust and 1-6% change in torque in different advance ratios according to Table 9. This means that the flexibility of the propeller has improved its hydrodynamic performance. Displacement along the flow direction and pressure around the propeller at J=0.5 are illustrated in Fig. 14 and 15, respectively. As is clear form figure in suction side pressure is negative and in pressure side pressure is positive and that the deformation of the blade affects the pressure distribution. These are occurred by the inconsistency of deformed blade shape (Fig. 14) due to the difference in pressure distribution on the blade surface, especially near the blade tip zone, because the tip of propeller blade deformed mostly due to hydrodynamic force (Fig. 15).

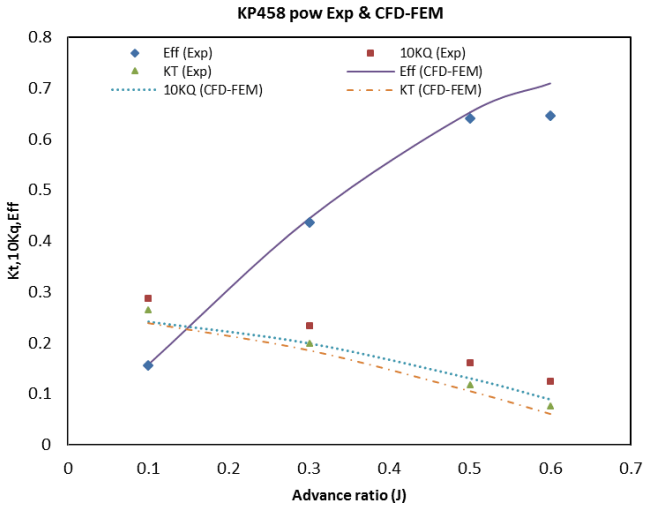

Figure. 13. Comparison of the hydrodynamic performances of KP458 POW composite propeller (CFD-FED) and rigid propeller (HMRI [23]).

Table 8. Difference between experimental and CFD-FEM values of KP458 (POW) test;

J	Exp			CFD-FEM			Error of Eff %
	KT (Exp)	10KQ (Exp)	Eff (Exp)	KT (CFD-FEM)	10KQ (CFD-FEM)	Eff (CFD-FEM)	
0.1	0.2654	0.2876	0.156	0.2389	0.2418	0.158	1.28%
0.3	0.1994	0.2335	0.436	0.1853	0.1993	0.444	1.83%
0.5	0.1173	0.1614	0.641	0.105	0.1306	0.652	1.73%
0.6	0.0756	0.1252	0.646	0.06	0.089	0.709	8.88%

Table 9. Thrust and torque estimation results for CFD and CFD-FEM values;

	condition		CFD		CFD-FEM		Thrust	torque
J	RPS	V (m/s)	Thrust (N)	Torque (N.m)	Thrust (N)	Torque (N.m)	change	change
0.1	0.5	0.046987	0.1056	0.00102	0.1106	0.000957	4.5208	-6.1764
0.3		0.14096	0.0819	0.00081	0.0829	0.000789	1.158	-2.1086
0.5		0.234933	0.0464	0.00052	0.0473	0.000518	1.9027	-1.8939
0.6		0.28192	0.0265	0.00037	0.027	0.000351	1.8518	-6.3466

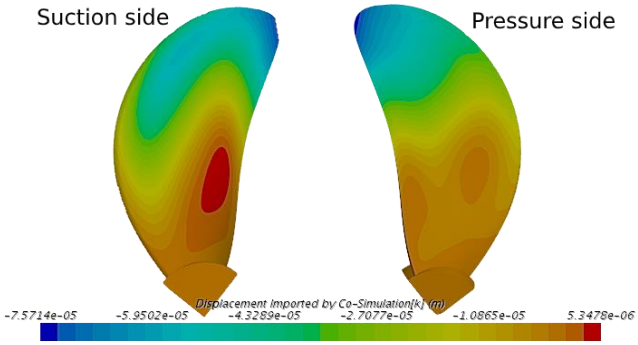

Figure. 14. Deformation distribution at J=0.5;

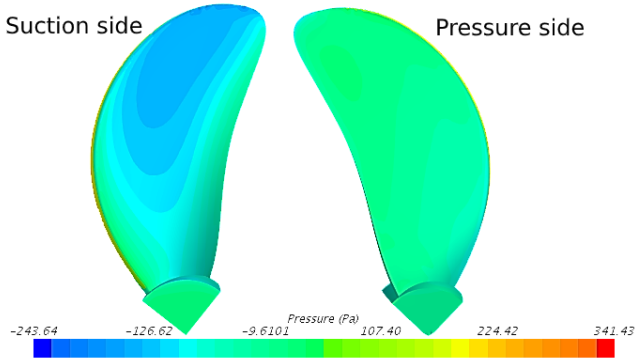

Figure. 15. Pressure distribution on flexible KP458 propeller surface at J=0.5 FSI simulation;

7. Conclusion

Composite propellers have many hydrodynamic, structural, and environmental advantages over conventional propellers. But for flexible propellers, hydrodynamic forces can cause deformations in the propeller geometry, which is essential for propeller efficiency. Therefore, this paper examines the hydroelastic performance of a composite propeller by using a 3D CFD-FEM numerical technique. Also, FSI analysis has been performed by the co-simulation technique with an implicit coupling scheme that allows fluid and structure solvers to exchange data more than once per time-step. The developed method has been validated by comparing the results with the EFD results of the benchmark four-bladed FPP propeller KP458.

A comparison was made between the two common methods for treating the propeller motion: sliding mesh and MRF. Also, two types of volume mesh were compared: polyhedral and hexahedral (trimmer). The results show more compatibility of MRF and polyhedral mesh with structural solver.

The results of the FSI analysis conducted in this study show an increase in the efficiency (increased thrust and decreased torque) of the composite propeller, which means reduced torque demand from the engine and thus lower fuel consumption. Therefore, composite propellers can be used for the development of a more efficient class of propulsion systems for commercial vessels, in the sense that they can improve fuel conservation.

8. References

1- Young, Y.L., (2007), *Time-dependent Hydro-elastic Analysis of Cavitating Propulsors*, Journal of Fluids and Structures, 23:269-295.

2- Mulcahy, N. L., Prusty, B. G. Gardiner, C. P., (2011) *Flexible composite hydrofoils and propeller blades*. Transactions of the Royal Institution of Naval Architects Part B: International Journal of Small Craft Technology, 153:39-46.

3- Mulcahy, N. L., Prusty, B. G. & Gardiner, C. (2010) *Hydroelastic tailoring of flexible composite propellers*. International Journal of Ship and Offshore Structures, 5:359-370.

4- Han, S., Lee, H., Song, M.C., Chang, B. J. *Investigation of hydro-elastic performance of marine propellers using fluid-structure interaction analysis*, ASME Int. Mech. Eng. Congr. Expo. Proc. 7A–2015.

5- Lee, H., Song, M.C., Han, S., Chang, B.-J., Suh, J.-C., (2017), *Hydro-elastic aspects of a composite marine propeller in accordance with ply lamination methods*, J. Mar. Sci. Technol. 22:479–493.

6- Lin, H.J., Lin, J.J. (1996), *Nonlinear hydroelastic behavior of propellers using a finite-element method and lifting surface theory*, J. Mar. Sci. Technol. 1:114–124.

7- Rao, Y.S., Rao, K.M., Reddy, B.S. (2012), *Stress Analysis of Composite Propeller By Using Finite Element Analysis*, Int. J. Eng. Sci. Technol. 4:3866–3875.

8- Lin, H.J., Lin, J.J., Chuang, T.J. (2005), *Strength evaluation of a composite marine propeller blade*, J. Reinf. Plast. Compos. 24:1791–1807.

9- Pavan Kishore, M.L., Behera, R.K., Bezawada, S., (2013), *Structural Analysis of NAB Propeller Replaced With Composite Material*, Int. J. Mod. Eng. Res. 3: 401–405.

10- Ghassemi, H., Fadavie, M., Nematy, D., (2015), *Hydro-Structure Analysis of Composite Marine Propeller under Pressure Hydrodynamic Loading*, Am. J. Mech. Eng. 3:41–46.

11- Paik, Bu-Geun & Kim, Gun-Do & Kim, Kyung-Youl & Seol, Han-Shin & Hyun, Beom-Soo & Lee, Sang-Gab & Jung, Young-Rae., (2013), *Investigation on the performance characteristics of the flexible propellers*. Ocean Engineering. 73:139-148. 10.1016/j.oceaneng.2013.09.005.

12- Lee, H., Song, M., Suh, J., Chang, B., (2014). *Hydro-elastic analysis of marine propellers based on a BEM-FEM coupled FSI algorithm*. International Journal of Naval Architecture and Ocean Engineering. 6. 10.2478/ijnaoe-2013-0198.

13- Hong, Y. & Hao, L.F. & Wang, P.C. & Liu, W.B. & Zhang, H.M. & Wang, R.G. (2014). *Structural Design and Multi-Objective Evaluation of Composite Bladed Propeller*. Polymers and Polymer Composites. 22. 275-282. 10.1177.

14- Han, S. Lee, H. Song, M. Chang, B. (2015). *Investigation of Hydro-Elastic Performance of Marine Propellers Using Fluid-Structure Interaction Analysis*. V07AT09A038. 10.1115/IMECE2015-51089.

15- Das, H. Nirjhar & Kapuria, Santosh. (2016). *on the use of bend–twist coupling in full-scale composite marine propellers for improving hydrodynamic performance*. Journal of Fluids and Structures. 61. 132-153. 10.1016/j.jfluidstructs.2015.11.008.

16- Hong, Y. & Wilson, Philip & He, X.D. & Wang, R.G. (2017). *Numerical analysis and performance comparison of the same series of composite propellers*. Ocean Engineering. 144. 211-223. 10.1016/j.oceaneng. 2017.08.036.

17- Kumar, A. Krishna, L. Subramanian, V. (2019). *Design and Analysis of a Carbon Composite Propeller for Podded Propulsion*. 10.1007/978-981-13-3119-0_13.

18- Zhang, F., & Ma, J. (2018). *FSI Analysis the Dynamic Performance of Composite Propeller*. V002T08A006. 10.1115/OMAE2018 77108.

19- Raja, V. & Venkatesan, K. & Kumar. M., Senthil & Kumar G, R. & Jagadeeshwaran, P. & Kumar, R., (2020), *Comparative fatigue life estimations of Marine Propeller by using FSI*. Journal of Physics: Conference Series. 1473. 012018.

20- Young YL. (2008), *Fluid-structure interaction analysis of flexible composite marine propellers*. J Fluids Struct 24:799–818.

21- Luhar, Mitul & Nepf, Heidi. (2011), *Flow-induced reconfiguration of buoyant and flexible aquatic vegetation*. Limnology and Oceanography. 56. 2003-2017. 10.4319/lo.2011.56.6.2003.

22. CD Adapco, (2017). STAR CCM+ User's Guide Version 12.04.010.

23- Sung, Y.J., Park, S-H., Ahn, K-S., Chung, S-H., Shin, S.S. and Jae-Hyoung, J. (2014), *Evaluation on Deep Water Manoeuvring Performances of KVLCC2 Based on PMM Test and RANS Simulation*, Hyundai Heavy Industries Co., Ltd and CD-Adapco Korea, Republic of Korea. Proceedings of SIMMAN.

24- ITTC-Recommended Procedures and Guidelines, (2008). Uncertainty Analysis in CFD Verification and Validation Methodology and Procedures. 7.5-03-01-01.

25- ITTC-Recommended Procedures and Guidelines, (2014). Practical Guidelines for Ship Self-Propulsion CFD. 7.5–03–03–01.